Soft Matter

COMMUNICATION

View Article Online
View Journal | View Issue

Cite this: *Soft Matter*, 2015, **11**, 8404

Received 15th August 2015,
Accepted 8th September 2015

DOI: 10.1039/c5sm02041g

www.rsc.org/softmatter

Bacterial transport of colloids in liquid crystalline environments†

Rishi R. Trivedi,[a] Rina Maeda,[a] Nicholas L. Abbott,[b] Saverio E. Spagnolie*[c] and Douglas B. Weibel*[ade]

We describe the controlled transport and delivery of non-motile eukaryotic cells and polymer microparticles by swimming bacteria suspended in nematic liquid crystals. The bacteria push reversibly attached cargo in a stable, unidirectional path (or along a complex patterned director field) over exceptionally long distances. Numerical simulations and analytical predictions for swimming speeds provide a mechanistic insight into the hydrodynamics of the system. This study lays the foundation for using cargo-carrying bacteria in engineering applications and for understanding interspecies interactions in polymicrobial communities.

The manipulation of microscale structures is an unsolved challenge in microengineering and microtechnology. One approach has been to harness the mechanical work performed by cells, which takes advantage of their metabolism and motility machinery to convert chemical energy to motion in a wide range of chemical and physical environments.[1] Extracellular sensors enable cells to adapt and navigate through different environments, thereby providing mechanisms to control their motion and the objects they are moving. The earliest examples of research in this area include the movement of polymer structures with length scales of hundreds of microns by bacterial cells adsorbed on the polymer surface,[2] and the guided transport and release of polymer colloids by individual phototactic, motile algae.[3] Related efforts have included magnetically-driven transport of cargo by synthetic swimmers with possible applications in targeted drug delivery.[4]

Bacteria have been the source of additional studies on microstructure transport as they are fast (velocities approaching ≈ 100 μm s^{-1}) and adaptable, genetic tools are widely available for engineering their properties and behavior, and a range of mechanisms can be exploited to control their motion, including: concentration gradients of ions and chemicals, magnetic fields, light, heat, oxygen, and redox potential.[5,6] Many rod-shaped bacteria swim through fluids by rotating their flagella in a counterclockwise direction to form a bundle and 'run'. Rotating a flagellum in the clockwise direction alters the structure of the bundle and reorients cells, which creates an event referred to as a 'tumble'. Controlling the motion of many flagellated bacteria is complicated by run and tumble dynamics;[7] accordingly, bacteria-based motility of microscale objects is highly challenging, as it is difficult to place objects on cells without disrupting and inhibiting normal cell behavior. Applications relying on chemotaxis to move small cargo pose similar challenges due to spatial and temporal instability of chemical gradients.[8] Confined domains such as microfluidic channels can also influence particle trajectories.[9]

A new method for directing bacterial motion without channels or gradients was recently developed, in which motile bacteria are suspended in solutions of nematic, lyotropic liquid crystals (LCs) consisting of disodium cromoglycate (DSCG).[10,11] In nematic LCs, bacteria were found to align with and swim along the nematic director field,[10–12] which suggests a new way to harness microorganisms as biological engines. A recent paper demonstrated that a bacterial cell swimming in a nematic LC can influence the position of polymer microspheres through long-range hydrodynamic interactions.[13]

In this Communication we describe the environmental relevance of the controlled transport and delivery of microparticles by swimming bacteria. We show that freely swimming *P. mirabilis* bacteria can push non-motile fungal cells in a stable, unidirectional path over long distances. By patterning a complex director profile in the fluid, the bacteria and cargo may be guided along a predefined path. Experiments with polymer microparticles, numerical simulations based on isotropic

[a] *Department of Biochemistry, University of Wisconsin-Madison, 440 Henry Mall, Madison, WI 53706, USA. E-mail: weibel@biochem.wisc.edu*
[b] *Department of Chemical and Biological Engineering, University of Wisconsin-Madison, 1415 Engineering Dr., Madison, WI 53706, USA*
[c] *Department of Mathematics, University of Wisconsin-Madison, 480 Lincoln Dr., Madison, WI 53706, USA. E-mail: spagnolie@math.wisc.edu*
[d] *Department of Chemistry, University of Wisconsin-Madison, 1101 University Ave., Madison, WI 53706, USA*
[e] *Department of Biomedical Engineering, University of Wisconsin-Madison, 1550 Engineering Dr., Madison, WI 53706, USA*

† Electronic supplementary information (ESI) available. See DOI: 10.1039/c5sm02041g

viscous flow, and analytical predictions for swimming speeds of cargo-pushing bacteria provide mechanistic insight and emphasize the importance of hydrodynamic interactions in the system. This study lays the foundation for using cargo-carrying bacteria in unique ways, from the bottom-up assembly of mesoscopic materials to the study of interspecies interactions in polymicrobial communities in anisotropic biological environments such as mucus and biofilms.

Experiments

It has been suggested that motile microorganisms may transport non-motile cells in different ecological niches to increase their adaptation, fitness, and survival.[6,14] Both *P. mirabilis* and the non-motile fungus *C. albicans* are opportunistic pathogens that are associated with urinary tract infections (UTI) and have been isolated from UTI patients.[15] The urinary tract is lined with a layer of mucus secreted by the urinary epithelium, which under conditions of external flow (*i.e.*, flow of fluid adjacent to the mucus) may align molecules to exhibit orientational order similar to nematic LCs and guide cell motion. Fluid anisotropy has also been reported in cervical mucus due to the ordering of parallel strands of polymers,[16] which may guide sperm cells entering the cervical canal to follow the mucus 'director'.[17] We used the nematic LC to mimic the physical properties of the epithelial mucus and study whether *P. mirabilis* cells push *C. albicans* cells in long-range, rectified motion in a simple mechanical model of the mammalian urinary tract.

As a model anisotropic fluid we used aqueous solutions of 15 wt% DSCG due to its biocompatibility with bacteria.[18] DSCG forms nematic-phase LCs at room temperature which is well suited for bacterial growth and motility.[19] An isotropic phase of DSCG was achieved by heating the sample to 30 °C. For our studies we used *P. mirabilis* strain HI4320 (with cell body widths $\approx$0.5 μm and lengths $\approx$2–3 μm), a clinical isolate collected from an elderly patient with a long-term in-dwelling urinary catheter.[20] We engineered cells to overexpress the flhDC operon, which encodes the master regulator of flagella biosynthesis, FlhD4C2 to match the density of flagella expressed by *P. mirabilis* swarmer cells implicated in urinary tract infections (UTIs).[21]

We mixed motile *P. mirabilis* cells with non-motile *C. albicans* cells (5 μm in diameter) and suspended them in $\approx$20 μm-thick nematic LC sandwiched between two rubbed coverslips, and imaged cell behavior using phase contrast microscopy (Fig. S1, ESI†). Single *P. mirabilis* cells pushed *C. albicans* cells along the far-field director with a speed of $\approx$1–2 μm s^{-1}, which is fast enough to disperse yeast cells to relatively long distances of $\approx$5 mm over the course of an hour (Fig. 1a). We then engineered a 'complex' LC director profile by rubbing the glass in a curved pattern and observed motile *P. mirabilis* cells pushing *C. albicans* cells over distances of hundreds of microns that followed the director (Fig. 1b, Fig. S3, ESI†). In addition to individual *P. mirabilis* cells pushing single *C. albicans* cells, we also observed multiple bacterial cells pushing groups of a group of fungal cells. In these experiments, the nematic LC promotes

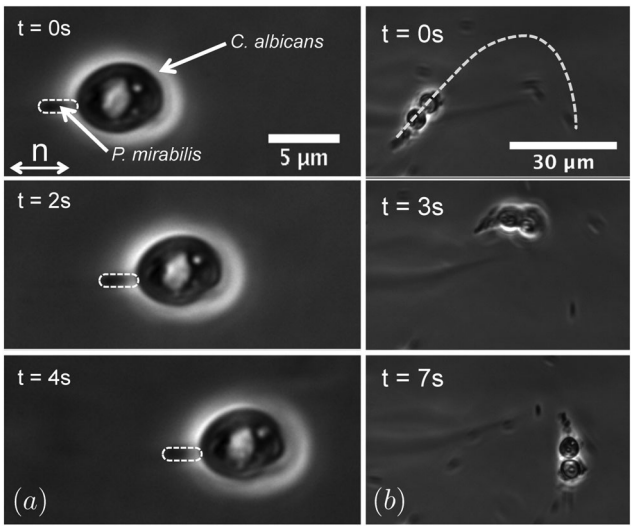

Fig. 1 (a) A single *P. mirabilis* cell pushes a single *C. albicans* cell along the far-field nematic LC director (**n**) (see Movie S1, ESI†). (b) Multiple *P. mirabilis* cells pushing a group of *C. albicans* cells along curved path following the director profile, which is indicated by the dashed line (see Movie S2, ESI†).

particle/particle interactions (between *P. mirabilis* and *C. albicans*), active particles provide the mechanical work for movement along the LC director, and passive particles provide a physical barrier that inhibits bacterial cell tumbling that would ordinarily lead to direction reversal. Consequently the pair of *P. mirabilis* and *C. albicans* cells are locked in a long-range motile run in LCs that eclipses the net distance achievable by either of the individual cells.

To better understand cargo transport in a more controlled experiment, we mixed *P. mirabilis* cells and 2 μm-diameter polystyrene microparticles, and observed many cells pushing microparticles along the far-field nematic director over long distances (Fig. 2). Microparticles were always positioned at the 'front' of (and pushed by) the motile cells. In a typical experiment we used a stoichiometry of 1 : 1 ratio of cells : particles and observed $\approx$10–15% of the cells moving particles at a mean velocity of $\approx$5 μm s^{-1}. In an isotropic LC, individual *P. mirabilis* cells were in contact with 2 μm-diameter microparticles for a

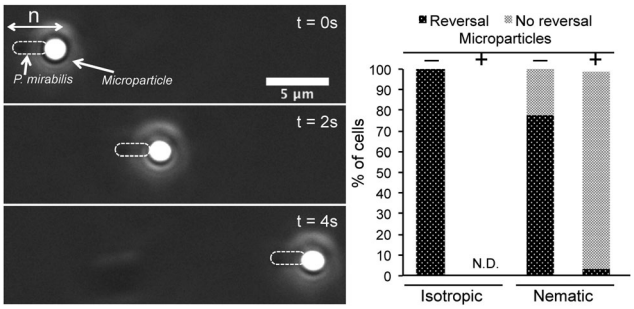

Fig. 2 (Left) Timelapse of a single *P. mirabilis* cell pushing a 2 μm-diameter polystyrene microparticle along the far-field nematic LC director (**n**) (see Movie S3, ESI†). (Right) Percentage of cells reversing in isotropic and in nematic LC in the absence (–) or presence (+) of microparticles. N.D.: not determined.

"carry" time (mean run time with the cargo) of 0.18 ± 0.1 s, whereas in a nematic LC, the carry time was 460 ± 50 s, corresponding to transport distances of nearly 2000 body lengths. The elasticity of the LC environment inhibits bacterial reorientation, leading to robust particle transport.

Elastic forces exerted on suspended particles in nematic LCs can explain differences in the carry time in isotropic and nematic phases. Mechanical anisotropy of the nematic LC aligns cells with their long-axis parallel to the far-field director profile. When cells in a nematic LC 'tumble', their swimming direction changes by 180°.[10] We compared the frequency of cell reversals in isotropic and nematic LCs (for 100 cells) and observed 100% of the cells in the isotropic LC tumble multiple times over a 5 minute timeframe compared to 78% cells in a nematic LC (180° reversal). This reduction from 100% to 78% can be rationalized in terms of the extra elastic forces on the flagellum due to the environmental anisotropy:[22] the flagellar bundle is likely unable to splay and cause cell body reorientation in a viscoelastic medium. Reversals in a nematic LC are then primarily driven by the competing activity of two flagellar bundles on opposite sides of the cell body. However, when the bacteria in the nematic LC were pushing 2 μm-diameter microparticles, we observed a dramatic drop in the number of reversing cells during the same timeframe to only 3% (Fig. 2). This more pronounced decrease may be due to the flagellar bundle positioned at the front of the cell (in contact with the microparticle) becoming non-functional.

We also studied the bacterial transport of microparticles of different sizes to probe the relative flagellar forces and resultant swimming speeds. Fig. 3a shows the swimming speeds using microparticles ranging from 1–3 μm in diameter (shown as circles with standard error bars). With no microparticle load the mean swimming speed of *P. mirabilis* was 9.6 μm s^{-1}. Upon the addition of microparticles, the speeds decreased monotonically with increasing particle size, to values 7.2, 5.2, and 1.5 μm s^{-1} for diameters 1, 2, and 3 μm. Fluctuations in the swimming speed were observed on a short timescale (the normal timescale of tumbling events) and over a longer timescale (time series examples are provided in the Fig. S4, ESI†). Swimming speeds while pushing a 2 μm-diameter microparticle fluctuated with a standard deviation of approximately 1.35 μm s^{-1}, suggesting a time ≈1 s beyond which the distance travelled due to the mean swimming speed dominates the distance travelled due to fluctuations. The nonlinear progression of motion shown in Fig. 2 is associated with such fluctuations.

Mathematical model

While the fluid anisotropy in the experiments clearly results in alignment and stability of the system, we studied a mathematical model describing a simpler isotropic viscous flow, the Stokes equations, $\nabla p = \mu\nabla^2\mathbf{u}$, $\nabla\cdot\mathbf{u} = 0$, where $\mathbf{u}$ is the fluid velocity, μ is the viscosity, and p is the pressure. Inertial forces are dominated by viscous forces in flows relevant to microorganism locomotion.[23] A fundamental (Green's function) solution to these equations, associated with the placement of a point force in an infinite quiescent fluid at a point $\mathbf{x}_0$, is known as the Stokeslet,

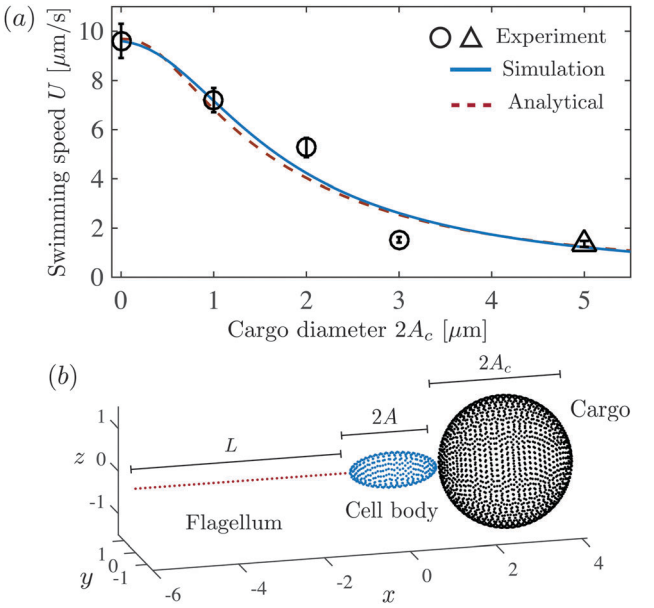

Fig. 3 (a) Swimming speed for a range of cargo sizes, from experiments (circles – microbeads; triangle – *C. albicans* cell), numerical simulation (solid line), and analytical prediction (dashed line). (b) Model microorganism with spherical cargo.

$8\pi\mu\mathbf{u}(\mathbf{x}) = \mathbf{G}(\mathbf{x}, \mathbf{x}_0)\cdot\mathbf{f}$, where $\mathbf{G}(\mathbf{x}, \mathbf{x}_0) = (r^{-1}\mathbf{I} + r^{-3}\mathbf{rr})$, where $\mathbf{I}$ is the identity, $\mathbf{r} = \mathbf{x} - \mathbf{x}_0$, and $r = |\mathbf{r}|$.[24] The cell body and microparticle are discretized uniformly in space, (see Fig. 3b); to model the flagellum we follow ref. 25 and represent the averaged forcing as a uniform line distribution of Stokeslets.

To compute the full hydrodynamics we employ the method of regularized Stokeslets,[26] wherein smoothed versions of the singular solution are distributed over the surfaces of the model cell body and microparticle, with strengths determined so that the no-slip velocity boundary condition is satisfied. The equations are closed by requiring the net force on the system to be zero, a consequence of neutrally buoyant locomotion at small length scales.[23] Further details about the numerical method are included in the ESI.†

We used experimentally motivated parameters: a cell body with length $2A$ = 2 μm, width $2B$ = 0.8 μm, flagellum length L = 5 μm, and microparticle radii $A_c \in [0,2.5]$ μm. The model requires a single fitted parameter, the force F generated by the flagellum, which we selected so that the swimming speed of the model microorganism with no microparticle matches the experimentally measured value, U = 9.6 μm s^{-1}. Using the measured viscosity, μ = 0.7 Pa s, this requisite flagellar force is computed to be F = 134.5 pN, which is comparable to the elastic forces and flagella-derived forces measured in previous experiments.[10]

The results of the numerical simulations are shown as a solid line in Fig. 3a, where the model clearly shows the trend of decreasing speed with increasing microparticle sizes. The agreement between the experiments and the numerical simulation, even using the isotropic Stokes equations, is reasonable, save for the notable overestimation of the speed for the cargo of diameter 3 μm. The numerical simulations are highly suggestive of the importance of hydrodynamic interactions between

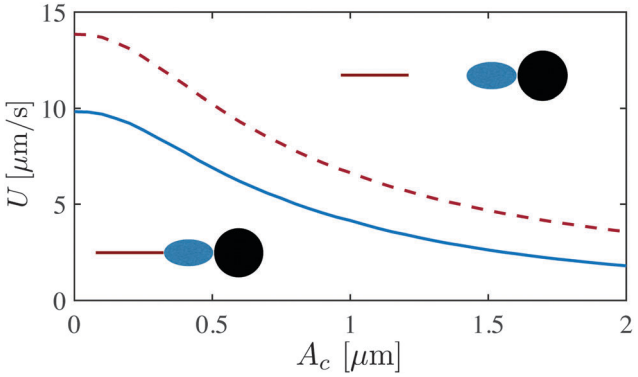

Fig. 4 Computed speed of a cell-body and cargo driven by a nearby flagellum (solid line) and a very distant flagellum (dashed line), underscoring the importance of hydrodynamic interactions.

the flagellum and the cell body/cargo load. Fig. 4 shows the speed of the total load as driven by an attached flagellum (solid line) and by a very distant flagellum (dashed line). The predicted swimming speed can be remarkably different; similarly, any estimate of the flagellar force imposed onto such a load may be inaccurate if hydrodynamic interactions are not included.

The mathematical model also offers the possibility of finding an analytical prediction of the swimming speed for variable cargo sizes, cell body shapes, and flagellum lengths. An estimate which includes the leading order hydrodynamic interactions in a far-field calculation (see ESI†) results in the swimming speed U of the model microorganism with no microparticle given by

$$\left(\frac{6\pi\mu A K_e}{F}\right) U = 1 - \frac{3K_e}{2+\lambda}, \tag{1}$$

where $K_e = 8e^3(-6e + 3(1 + e^2)\log[(1 + e)/(1 - e)])^{-1}$ and $e = \sqrt{1-(B/A)^2}$. The second term on the right hand side modifies the drag coefficient on the cell body due to the flow from the flagellum. Related techniques have been used to study the hydrodynamics of locomotion near surfaces and colloidal obstacles.[25,27] Using the same geometric parameters as before, we again fit the flagellar force F to match the experimental swimming speed of the cargo-less body, which in the simpler analytical model requires $F = 98.3$ pN. When a microparticle is introduced, we find a more general relation,

$$\left(\frac{6\pi\mu A}{F}\right) U = \frac{C(\kappa,\lambda)}{D(\kappa,\lambda)}, \tag{2}$$

where

$$C(\kappa,\lambda) = 4(\kappa+1)^2(\lambda+2)(4+\lambda-\kappa) + 3K_e\{\kappa(4(\kappa^2+\kappa-7) + 2(\kappa-7)\lambda - 3\lambda^2) - 4(\lambda+4)\}, \tag{3}$$

$$D(\kappa,\lambda) = 4(\kappa+1)(\lambda+2)(2\kappa+\lambda+4)\,(\kappa^2+\kappa-2\kappa K_e + K_e), \tag{4}$$

with $\kappa = A_c/A$ and $\lambda = L/A$. The analytical prediction from eqn (2) is included as a dashed line in Fig. 3a, showing a very clear connection to the full numerical simulations. While the isotropic model provides useful predictions in this case, the mathematical investigation of locomotion in anisotropic fluids has only recently seen attention[28] and there is a need for further study in this direction.

Discussion

We have demonstrated that motile bacterial cells can transport polymer microparticles and non-motile cells unidirectionally along the far-field director in lyotropic nematic LCs. There are several conclusions to be drawn from this study. (1) The LC facilitates the interaction between bacterial cells and non-motile objects, and brings them into close physical proximity while avoiding irreversible adsorption and attachment. (2) The mechanical anisotropy of a nematic LC guides the cell pushing loads along the far-field director, and the load inhibits cell reversal. (3) Non-motile organisms and cells can catch a ride on motile bacteria, suggesting a possible host invasion strategy exploited by non-motile microorganisms hitchhiking in fluidic environments. (4) Instead of using tethering assays,[29] the study suggests a novel means of measuring mechanosensing responses by changing the size and shape of the passive load. (5) This method of microscale transport and manipulation is in principle material independent (*e.g.*, polymers, silica, and cells) and does not require the engineering of cells or materials. (6) Motile bacteria may be useful as a tracer of the complex LC director profile in nematic LCs. (7) In LCs, particles are positioned at the front end of motile bacterial cells, which reduces their interference with the bundle of rotating flagella used to propel bacteria. This study demonstrates an approach for controlling the transport of microscope objects using motile bacterial cells that may have applications that range from the bottom-up assembly of materials to the study of interspecies interactions in polymicrobial communities that occur in LC-like environments, such as biofilms.

Acknowledgements

This work was supported by the National Science Foundation (under awards DMR-1121288 (MRSEC), CBET-0754921, and MCB-1120832), the National Institutes of Health (CA108467 and AI092004), and the United States Department of Agriculture (WIS01594).

References

1 J. G. Mitchell and G. M. Barbara, *Aquat. Microb. Ecol.*, 1999, **18**, 227–233.
2 N. Darnton, L. Turner, K. Breuer and H. C. Berg, *Biophys. J.*, 2004, **86**, 1863–1870; Y. Hiratsuka, M. Miyata, T. Tada and T. Q. P. Uyeda, *Proc. Natl. Acad. Sci. U. S. A.*, 2006, **103**, 13618–13623.
3 D. B. Weibel, P. Garstecki, D. Ryan, W. R. DiLuzio, M. Mayer, J. E. Seto and G. M. Whitesides, *Proc. Natl. Acad. Sci. U. S. A.*, 2005, **102**, 11963–11967.
4 O. S. Pak, W. Gao, J. Wang and E. Lauga, *Soft Matter*, 2011, **7**, 8169–8181; W. Gao, D. Kagan, O. S. Pak, C. Clawson,

S. Campuzano, E. Chuluun-Erdene, E. Shipton, E. E. Fullerton, L. Zhang, E. Lauga and J. Wang, *Small*, 2012, **8**, 460–467; E. E. Keaveny, S. W. Walker and M. J. Shelley, *Nano Lett.*, 2013, **13**, 531–537.

5 A. Sokolov, M. M. Apodaca, B. A. Grzybowski and I. S. Aranson, *Proc. Natl. Acad. Sci. U. S. A.*, 2010, **107**, 969–974; R. Fernandes, M. Zuniga, F. R. Sassine, M. Karakoy and D. H. Gracias, *Small*, 2011, **7**, 588–592.

6 A. Shklarsh, A. Finkelshtein, G. Ariel, O. Kalisman, C. Ingham and E. Ben-Jacob, *Interface Focus*, 2012, **2**, 786–798.

7 H. C. Berg, *Random Walks in Biology*, Princeton University Press, 1993.

8 A. Sahari, M. A. Traore, B. E. Scharf and B. Behkam, *Biomed. Microdevices*, 2014, **16**, 717–725.

9 W. R. DiLuzio, L. Turner, M. Mayer, P. Garstecki, D. B. Weibel, H. C. Berg and G. M. Whitesides, *Nature*, 2005, **435**, 1271–1274; S. E. Hulme, W. R. DiLuzio, S. S. Shevkoplyas, L. Turner, M. Mayer, H. C. Berg and G. M. Whitesides, *Lab Chip*, 2008, **8**, 1888–1895; J. L. Connell, A. K. Wessel, M. R. Parsek, A. D. Ellington, M. Whiteley and J. B. Shear, *mBio*, 2010, **1**, e00202.

10 P. C. Mushenheim, R. R. Trivedi, H. H. Tuson, D. B. Weibel and N. L. Abbott, *Soft Matter*, 2014, **10**, 79–86.

11 S. Zhou, A. Sokolov, O. D. Lavrentovich and I. S. Aranson, *Proc. Natl. Acad. Sci. U. S. A.*, 2014, **111**, 1265–1270.

12 A. Kumar, T. Galstian, S. Pattanayek and S. Rainville, *Mol. Cryst. Liq. Cryst.*, 2013, **574**, 33–39.

13 A. Sokolov, S. Zhou, O. D. Lavrentovich and I. S. Aranson, *Phys. Rev. E: Stat., Nonlinear, Soft Matter Phys.*, 2015, **91**, 013009.

14 J. A. Warmink and J. D. van Elsas, *Appl. Environ. Microbiol.*, 2009, **75**, 2820–2830; C. J. Ingham, O. Kalisman, A. Finkelshtein and E. Ben-Jacob, *Proc. Natl. Acad. Sci. U. S. A.*, 2011, **108**, 19731–19736; J. A. Warmink, R. Nazir, B. Corten and J. D. van Elsas, *Soil Biol. Biochem.*, 2011, **43**, 760–765; M. Pion, J. E. Spangenberg, A. Simon, S. Bindschedler, C. Flury, A. Chatelain, R. Bshary, D. Job and P. Junier, *Proc. Biol. Sci.*, 2013, **280**, 2242; R. Moscaritolo, M. Kinley, A. Raegen, M. Giuliani, R. White, C. Kelly, L. L. Burrows and J. R. Dutcher, *Phys. in Can.*, 2013, **69**, 137–139; A. Finkelshtein, D. Roth, E. Ben Jacob and C. J. Ingham, *mBio*, 2015, **6**, e00074.

15 R. Orenstein and E. S. Wong, *Am. Fam. Physician*, 1999, **59**, 1225–1234; L. E. Nicolle and A. C. G. Committee, *Can J Infect Dis Med Microbiol*, 2005, **16**, 349–360.

16 C. Viney, A. E. Huber and P. Verdugo, *Macromolecules*, 1993, **26**, 852–855; L. S. M. A. Fritz, *Clinical Gynecologic Endocrinology and Infertility*, Lippincott Williams & Wilkins, 8th edn, 2011, p. 1.

17 F. C. Chretien, *Acta Obstet. Gynecol. Scand.*, 2003, **82**, 449–461.

18 N. H. Hartshorne and G. D. Woodard, *Mol. Cryst. Liq. Cryst.*, 1981, **64**, 153–154; H. Lee and M. M. Labes, *Mol. Cryst. Liq. Cryst.*, 1983, **91**, 53–58.

19 L. L. Cheng, Y. Y. Luk, C. J. Murphy, B. A. Israel and N. L. Abbott, *Biomaterials*, 2005, **26**, 7173–7182.

20 H. L. T. Mobley and R. Belas, *Trends Microbiol.*, 1995, **3**, 280–284.

21 H. H. Tuson, M. F. Copeland, S. Carey, R. Sacotte and D. B. Weibel, *J. Bacteriol.*, 2013, **195**, 368–377.

22 I. Musevic, M. Skarabot, U. Tkalec, M. Ravnik and S. Zumer, *Science*, 2006, **313**, 954–958.

23 E. Lauga and T. Powers, *Rep. Prog. Phys.*, 2009, **72**, 096601.

24 C. Pozrikidis, *Boundary Integral and Singularity Methods for Linearized Viscous Flow*, Cambridge University Press, Cambridge, UK, 1992.

25 S. E. Spagnolie and E. Lauga, *J. Fluid Mech.*, 2012, **700**, 1–43.

26 R. Cortez, *SIAM J. Sci. Comput.*, 2001, **23**, 1204–1225; J. Ainley, S. Durkin, R. Embid, P. Boindala and R. Cortez, *J. Comput. Phys.*, 2008, **227**, 4600–4616.

27 A. P. Berke, L. Turner, H. C. Berg and E. Lauga, *Phys. Rev. Lett.*, 2008, **101**, 038102; R. Di Leonardo, D. Dell'Arciprete, L. Angelani and V. Iebba, *Phys. Rev. Lett.*, 2011, **106**, 038101; D. Lopez and E. Lauga, *Phys. Fluids*, 2014, **26**, 071902; S. E. Spagnolie, G. R. Moreno-Flores, D. Bartolo and E. Lauga, *Soft Matter*, 2015, **11**, 3396–3411.

28 M. S. Krieger, S. E. Spagnolie and T. R. Powers, *Phys. Rev. E: Stat., Nonlinear, Soft Matter Phys.*, 2014, **90**, 052503; M. S. Krieger, M. A. Dias and T. R. Powers, arXiv preprint arXiv:1506.01696, 2015; M. S. Krieger, S. E. Spagnolie and T. R. Powers, arXiv preprint arxiv:1507.00776, 2015.

29 P. P. Lele, B. G. Hosu and H. C. Berg, *Proc. Natl. Acad. Sci. U. S. A.*, 2013, **110**, 11839–11844.

